

X-ray and Optical Observations of the Black Hole Candidate MAXI J1828–249

Sonoe ODA,^{1,2,*} Megumi SHIDATSU,^{3,4} Satoshi NAKAHIRA,³ Toru TAMAGAWA,^{1,2} Yuki MORITANI,^{5,6} Ryosuke ITOH,^{7,8} Yoshihiro UEDA,⁹ Hitoshi NEGORO,¹⁰ Kazuo MAKISHIMA,^{3,5} Nobuyuki KAWAI,^{3,7} and Tatehiro MIHARA³

¹RIKEN Nishina Center, 2-1 Hirosawa, Wako, Saitama 351-0198, Japan

²Department of Physics, Tokyo University of Science, 3-1 Kagurazaka, Shinjuku-ku, Tokyo 162-8601, Japan

³MAXI team, RIKEN, 2-1 Hirosawa, Wako, Saitama 351-0198, Japan

⁴Department of Physics, Ehime University, 2-5 Bunkyocho, Matsuyama, Ehime 790-8577, Japan

⁵Kavli Institute for the Physics and Mathematics of the Universe (WPI), The University of Tokyo, 5-1-5 Kashiwanoha, Kashiwa, Chiba 277-8583, Japan

⁶Hiroshima Astrophysical Science Center, Hiroshima University, Higashi-Hiroshima, Hiroshima 739-8526, Japan

⁷Department of Physics, School of Science, Tokyo Institute of Technology, 2-12-1 Ohokayama, Meguro, Tokyo 152-8551, Japan

⁸Department of Physical Science, Hiroshima University, Kagamiyama 1-3-1, Higashi-Hiroshima 739-8526, Japan

⁹Department of Astronomy, Kyoto University, Kitashirakawa-Oiwake-cho, Sakyo-ku, Kyoto 606-8502, Japan

¹⁰Department of Physics, Nihon University, 1-8-14 Kanda-Surugadai, Chiyoda-ku, Tokyo 101-8308, Japan

*E-mail: sonoe.oda@riken.jp

Received ; Accepted

Abstract

We report results from X-ray and optical observations of the Galactic black hole candidate MAXI J1828–249, performed with Suzaku and the Kanata telescope around the X-ray flux peak in the 2013 outburst. The time-averaged X-ray spectrum covering 0.6–168 keV was approximately characterized by a strong multi-color disk blackbody component with an inner disk temperature of ~ 0.6 keV, and a power-law tail with a photon index of ~ 2.0 . We detected an additional structure at 5–10 keV, which can be modelled neither with X-ray reflection on the disk, nor relativistic broadening of the disk emission. Instead, it was successfully reproduced with a Comptonization of disk photons by thermal electrons with a relatively low temperature ($\lesssim 10$ keV). We infer that the source was in the intermediate state, considering its long-term trend in the hardness intensity diagram, the strength of the spectral power-law tail, and its variability properties. The low-temperature Comptonization component could be produced in a boundary region between the truncated standard disk and the hot inner flow, or a Comptonizing region that somehow developed above the disk surface. The multi-wavelength spectral energy distribution suggests that the optical and UV fluxes were dominated by irradiated outer disk emission.

Key words: accretion, accretion disks — black hole physics — X-rays: binaries — X-rays: individual (MAXI J1828–249)

1 Introduction

Black hole binaries (BHBs), consisting of a star and a stellar-mass black hole, are known to show various “states” with different X-ray properties (see e.g., Done et al. 2007 for reviews). The two most canonical ones are the “high/soft state” and “low/hard state”. The former is generally seen at high mass accretion rates, where the X-ray spectrum is dominated by soft X-rays produced as multi-temperature blackbody radiation from a standard accretion disk (Shakura & Sunyaev 1973). Many previous studies showed that the inner disk radius is kept fairly constant during the high/soft state (e.g., Makishima et al. 1986; Ebisawa et al. 1993; Steiner et al. 2010; Shidatsu et al. 2011); this suggests that the standard disk stably extends down to the innermost stable circular orbit (ISCO). The low/hard state is observed at relatively low mass accretion rates, where the X-ray spectrum is approximated by a power-law model with a photon index of <2 , often accompanied by an exponential cutoff at ~ 100 keV. It has been suggested that the standard disk in the low/hard state is truncated at a radius considerably larger than the ISCO, and turns into a radiatively inefficient hot accretion flow toward the vicinity of the central black hole (Esin et al. 1997; Makishima et al. 2008; Tomsick et al. 2009; Shidatsu et al. 2011, 2013). The hard power-law component is regarded as a result of inverse Compton scattering between the soft X-rays from the truncated standard disk, and hot electrons in some optically-thin zones, including in particular the regions inside the truncation radius, of the accretion flow (e.g., Poutanen 1998; Zdziarski et al. 1998; but see Reig et al. 2003; Markoff et al. 2005 for interpretations with jets). Properties of short-term variability also depend on the spectral states. In the low/hard state, BHBs show strong X-ray intensity variations, of which the power spectra usually consist of “band-limited noise” from ~ 0.1 Hz to 10–100 Hz, sometimes accompanied by quasi periodic oscillations at its high frequency edge (see e.g., Axelsson & Done 2018). These strong variations are suppressed in the high/soft state, wherein the standard disk is considered to fully develop down to the ISCO.

Even though previous observations in these two states have provided rich information, the structure of the black hole accretion flows and its evolution are not yet fully understood. One of the long-standing mysteries is the origin of the power-law “hard tail” seen above ~ 10 keV in the high/soft state spectra. Usually, it has a photon index of about $\gtrsim 2.1$ (McClintock & Remillard 2006), which is larger (steeper) than that of the X-ray continuum in the low/hard state, and does not show an exponential cut-off. If the hard tail is also produced by Comptonization of

the photons from the standard disk, the Comptonizing electrons are suggested to be much hotter than those in the low/hard state, or have a non-thermal distribution (e.g., Gierlinski et al. 1999). We do not either know whether the Comptonized continuum in the low/hard state continuously evolves into the hard tail in the high/soft state, or they are of different origins, and if the former is the case, how one evolves into the other and what drives that evolution. Observations in the transitional phases between these two states, collectively called the intermediate state, may provide clues to these questions.

As a system evolves from the low/hard state to the intermediate state, the power-law component in the hard X-ray band steepens, and the disk blackbody component gradually increases its fraction to the total X-ray flux. This is often explained by changes in the disk truncation radius; as the disk develops inwards and thereby the number of seed photons increases, the Comptonizing hot electrons are more efficiently cooled (e.g., Done et al. 2007; Sobolewska et al. 2011). However, how the physical structure of the Comptonization component evolves through in the intermediate state, and how it is connected to the hard tail in the high/soft state, are still unclear. In addition, the stability and typical duration of the intermediate state remain as another open question.

Observing the intermediate state is also important in understanding the physical mechanisms of outflows. The emission from compact jets seen in the low/hard state is suppressed after the transition to the high/soft state, whereas the absorption lines from disk winds behave in opposite ways (Ponti et al. 2012). This indicates that these outflows are also state-sensitive phenomena. However, the exact timing of their appearance/disappearance is not yet clear. The intermediate state may also provide a key to understanding the hysteresis of the state transition; the transition from the low/hard state to the high/soft state (the hard-to-soft transition) usually occurs at a considerably higher luminosity than the transition in the reverse direction (the soft-to-hard transition). Thus, through their outbursts, BHBs draw counter-clockwise, “q”-shaped tracks in their hardness-intensity diagrams (Homan & Belloni 2005), although different tracks are seen in some cases (e.g., Nakahira et al. 2014).

MAXI J1828–249 is a BHB candidate discovered with the Gas Slit Camera (GSC; Mihara et al. 2011) onboard MAXI (Monitor of All-sky X-ray Image; Matsuoka et al. 2009), on 2013 October 15 UT 21:55 (Nakahira et al. 2013), through the MAXI nova alert system (Negoro et al. 2016). Since its discov-

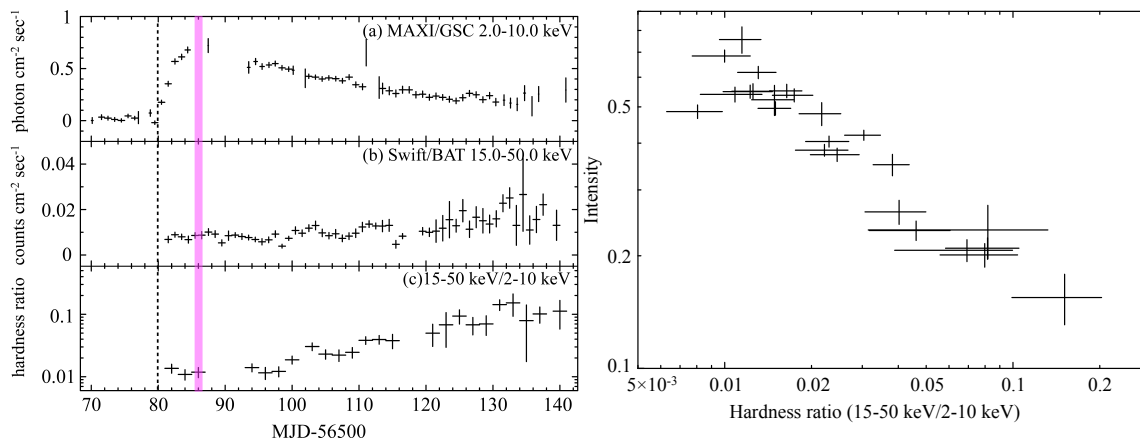


Fig. 1. Left: Long-term light curves of MAXI J1828–249 in 2–20 keV (panel a) and 15–50 keV (panel b), obtained with the MAXI/GSC and the Swift/BAT, respectively, and the hardness ratio between the 2–10 keV and 15–50 keV bands (panel c). Our Suzaku observation is indicated as the magenta stripe. The dashed line indicates the first MAXI detection and the start of spectral softening. MJD 56580 corresponds to 2013 October 15. Right: A hardness-intensity diagram created from the MAXI/GSC and Swift/BAT light curves over MJD 56580–56640.

ery, the source was extensively observed with MAXI, as well as Swift (Gehrels et al. 2004) and INTEGRAL (Winkler et al. 2003). The precise position was determined with the Swift/X-ray Telescope (XRT; Burrows et al. 2005) at $(\alpha^{2000}, \delta^{2000}) = (18^{\text{h}}28^{\text{m}}58.08^{\text{s}}, -25^{\circ}01'45''.3)$ (Kennea et al. 2013a, Negoro et al. 2016). A spectral softening was observed for several days after the MAXI discovery (Negoro et al. 2013; Kennea et al. 2013b; Krivonos & Tsygankov 2013). The optical and near-infrared counterpart was detected in that period, with apparent magnitudes of ~ 17 mag in the AB magnitude system, and the spectral energy distribution in the optical and near-infrared band were successfully explained by an outer disk emission (Rau et al. 2013). On 2013 October 21, 6 days after the spectral softening was first detected, we triggered a target-of-opportunity (ToO) observation of MAXI J1828–249 with Suzaku (Mitsuda et al. 2007), aiming at obtaining high-quality X-ray data of the target. We also carried out optical photometric observations with the Kanata telescope quasi-simultaneously with the Suzaku observation, to constrain the basic parameters of this system, such as the black hole mass, the distance, the type of the companion star, and the size of the accretion disk.

In the present paper, we describe the MAXI and Suzaku observations of MAXI J1828–249 (Section 2), analyze the Suzaku data (Section 3), and study broad-band spectral energy distribution (Section 4). Throughout the article, errors represent 90% confidence ranges, unless otherwise stated. We adopted the solar abundance table given by Wilms et al. (2000).

2 X-ray Observations

2.1 Long-term X-ray evolution in the outburst

Figure 1 shows the long-term X-ray light curves of the source in 2–20 keV and 15–50 keV, obtained with the MAXI/GSC and the

Swift/BAT, respectively, and the hardness ratio between them. After the discovery on 2013 October 15, the soft X-ray flux rapidly increased, and reached a peak in several days. In the meantime, the X-ray spectrum kept softening as detected with MAXI, Swift, and INTEGRAL (Kennea et al. 2013b; Negoro et al. 2013; Krivonos & Tsygankov 2013). It is hence suggested that the source was evolving through the low/hard state toward the high/soft state, even though a transition to the genuine high/soft state was not clearly recognized. X-ray spectra obtained in this period were characterized with a strong multi-color disk blackbody component and a power-law tail with a photon index of ~ 2 , seen mainly below and above ~ 10 keV, respectively (Filippova et al. 2014; Grebenev et al. 2016). Then, the flux gradually decreased for ~ 100 days down to undetectable levels. Meanwhile, the hardness ratio gradually increased, and then reached a maximum around MJD 56619, suggesting that the source returned to the low/hard state. Indeed, Tomsick & Corbel (2014) observed a power-law shaped spectrum, typical of the low/hard state, in a Swift observation performed ~ 4 months after the suggested first transition. Radio emission was not detected on MJD 56583, in the period of the X-ray spectral softening (Miller-Jones et al. 2013), but detected on MJD 56704, after the spectral hardening (Corbel et al. 2014). As shown in the right panel of figure 1, the source exhibited no significant hysteretic behavior in its hardness intensity diagram.

2.2 Suzaku Observation and Data Reduction

The Suzaku observation of MAXI J1828–249 was performed from 2013 October 21 UT 05:08:22 to October 22 UT 05:00:11 (OBSID=908002010). This was 6 days after the beginning of the spectral softening described in subsection 2.1. As shown in the left panel of figure 1, we caught the source in a brightest and softest phase in its 2013 outburst.

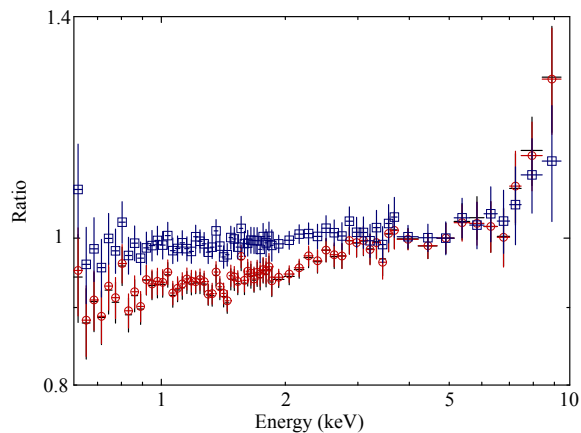


Fig. 2. Ratios of the background-subtracted XIS0 spectra extracted from a whole circular region ($r < 108''$, black crosses), the $r = 5''.6 - 108''$ annulus (red circles; with the pileup fraction of $< 3\%$), and the $r = 44'' - 108''$ annulus (blue squares; with $< 1\%$ pileup fraction), all divided by that from the $r = 70'' - 108''$ annulus. They are all normalized to unity at 5.0 keV.

Suzaku carries two X-ray instruments: the X-ray Imaging Spectrometer (XIS; Koyama et al. 2007) and the Hard X-ray Detector (HXD; Takahashi et al. 2007). The XIS is X-ray CCD cameras covering the soft X-ray band in the 0.2–12 keV range. In our observations, two cameras using front-side-illuminated chips (FI-XISs: XIS0 and XIS3) and one camera with back-side-illuminated configuration (BI-XIS: XIS1) were available. The HXD is a non-imaging, collimated hard X-ray detector composed of silicon PIN diodes and gadolinium silicon oxide (GSO) crystal scintillators, sensitive to 10–70 keV and 40–600 keV, respectively. Our observation was carried out in the XIS nominal position. The XIS was operated in the 1/4 window mode with the 0.1 s burst option, to avoid pile-up effects. The net exposure of the XIS was ≈ 2.5 ks, and those of PIN and GSO were ≈ 32 ks. The much shorter exposure of the XIS is due to the burst option.

The data reduction and analysis were carried out with HEASoft version 6.19 and Calibration Database released on 2016 April 24. We started the data reduction from the “cleaned” event files processed with the pipeline version 1.1.0, and followed the standard procedure described in the Suzaku data analysis manual¹. Source photons in the XIS data were extracted from a circular region with a radius of $108''$, centered on the target position. Following Yamada et al. (2012), we excluded the core of the point spread function with a radius of $44''$, so that the pile-up fraction was reduced to $< 1\%$. In fact, as shown in figure 2, the source spectrum accumulated over an annulus of $r = 44'' - 108''$ (r being the radius) has almost the same shape as that from a larger annulus of $r = 70'' - 108''$ (ratios in blue), although those from smaller inner radii (red for $r = 5''.6 - 108''$ and black for $r = 0'' - 108''$) exhibit shape distortion due to the pileup. Compared with the spectrum from the largest annulus of

$r = 70'' - 108''$, that from the $r = 44'' - 108''$ annulus still shows a slight difference above ~ 7 keV, which could be caused by the radial dependence of the response. This difference, however, has been confirmed not to affect the conclusion of this article. Background events were taken from a circle with a $90''$ radius in a blank-sky area. We have confirmed that the results presented in the following sections are unaffected by the choice of the position, size, and shape of the background region. We generated the response matrix files (RMFs) and ancillary response files (ARFs) of the individual XIS chips, using the HEASoft tool `xismrmfgen` and `xissimarfgen`, respectively.

Using the tools `hxdpinxblc` and `hxdpinxbpi`, we created a light curve and a spectrum of the PIN background, which consists of the cosmic X-ray background (CXB) and non X-ray background (NXB). The light curve and spectrum of the GSO background were made with `hxdgsoxblc` and `hxdgsoxbpi`, respectively. We ignored the CXB of GSO, because it contributes only 2 % of the total background. These products were obtained with the modelled NXB data provided by the Suzaku team². We adopted `ae_hxd_pinxinome11_20110601.rsp` to generate the RMF of PIN, and `ae_hxd_gsoxinom_20100524.rsp` and `ae_hxd_gsoxinom_crab_20100526.arf` for the RMF and ARF of GSO, respectively.

To assess the reproducibility of the NXB model of GSO, its prediction was compared with the data taken during Earth occultations of the target source in the actual observation. Then, in terms of the time averaged spectrum, as well as a 128 s bin light curve in 50–100 keV and that in 100–200 keV, the NXB model prediction agreed with the Earth occultation data, within the 1σ systematic errors given in Fukazawa et al. (2009). Specifically, the model-to-data ratios of the count rates, calculated every 128-s time interval, were found at 0.995 ± 0.006 and 1.000 ± 0.005 (where the errors represent 1σ standard errors over 143 data points) in 50–100 keV and 100–200 keV, respectively. Similarly, when the time averaged spectrum of the NXB model is compared with that of the occultation data, channel-by-channel ratios between the two spectra were obtained as 0.997 ± 0.006 in 50–100 keV and 0.998 ± 0.005 in 100–200 keV. Since the NXB model was thus confirmed to be reliable, and since it has higher statistics than the Earth occultation data, we selected the modeled NXB in subtracting the HXD-GSO background.

3 Analysis and Results of the Suzaku Data

3.1 Light Curves and Spectra

Figure 3 shows the background-subtracted Suzaku light curves of MAXI J1828–249 in 0.6–5 keV, 5–10 keV, 15–70 keV, and 50–200 keV. The former three light curves are binned in 128-s

¹ <https://heasarc.gsfc.nasa.gov/docs/suzaku/analysis/abc/>

² <http://www.astro.isas.jaxa.jp/suzaku/analysis/hxd/pinxb, gsoxb> (for the PIN and GSO NXB data, respectively)

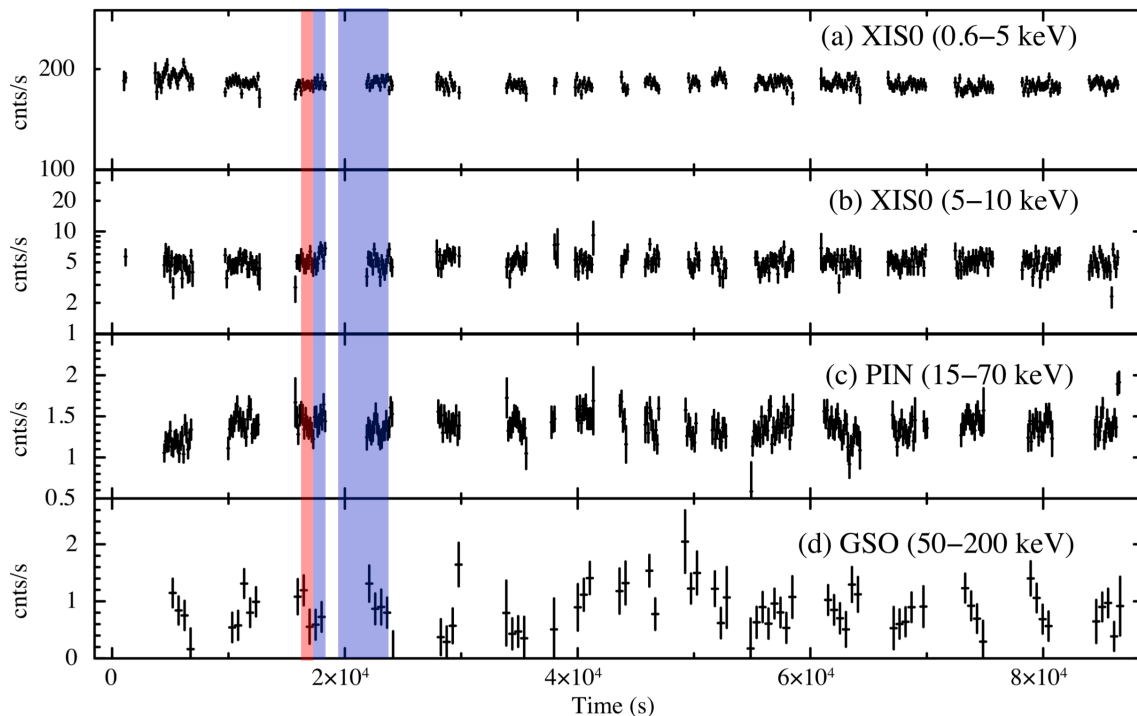


Fig. 3. Background-subtracted light curves of MAXI J1828–249 in 0.6–5 keV (panel a, with XIS0), 5–10 keV (panel b, the same), and 15–70 keV (panel c, HXD-PIN) with 128-s bins, and that in 50–200 keV (panel d, HXD-GSO) with 512-s bins. The HXD data were corrected for dead time. A red shaded region indicates the period of our optical *I*-band observations with the Kanata telescope, and blue regions those of the *R*-band observations. The XIS light curves employ logarithmic scales, whereas the HXD ones linear scales.

intervals, while the last one in 512 s bins to improve statistics. To quantitatively investigate intensity variation and its energy dependence, we calculated the excess variance σ_{rms}^2 , defined as (Vaughan et al. 2003)

$$\sigma_{\text{rms}}^2 = \frac{1}{N\bar{c}^2} \sum_{i=1}^N [(c_i - \bar{c})^2 - \sigma_i^2], \quad (1)$$

where N is the total number of the light curve points, \bar{c} is the mean count rate after the background subtraction, and c_i and σ_i are the count rate and its error at the i -th data point, respectively. Figure 4 presents an energy versus σ_{rms} plot, obtained from 128-s bin light curves in different energy bands within 0.6–200 keV. The σ_{rms} value is almost constant at ~ 0.05 in 5–70 keV, but it slightly decreases below 5 keV, to $\sigma_{\text{rms}} = 0.02$ –0.03. Thus, on time scales of 128 s to several tens ks, the source varied by $\sim 5\%$ in 5–70 keV, whereas 2–3% at lower energies. The GSO data in 50–200 keV provide only a weak upper limit as $\sigma_{\text{rms}} < 0.24$. Although the GSO light curve exhibits some hint of variation on time scales of ~ 10 ks, possibly correlated with systematic background changes, it is still within the statistical errors. Because of insufficient photon statistics of the HXD and the limited time resolution of the XIS, we were unable to extract any useful information on variations on shorter timescales of $\gtrsim 0.1$ Hz, where BHBs most prominently show their characteristic variations.

Figure 5 plots the time-averaged and background-subtracted spectra of XIS0–3, PIN, and GSO, derived over energy ranges of 0.6–10 keV, 15–70 keV, and 50–168 keV, respectively. For GSO, we employed the energy range where the source signals exceed 2% of the background level, considering the systematic uncertainty of the GSO background (subsection 2.2; Fukazawa et al. 2009). The data of the two FI-XIS cameras were combined in the following spectral analysis to improve statistics. We excluded the XIS data in 1.7–1.9 keV and 2.2–2.4 keV, because of the residual calibration uncertainties near the instrumental Si-K edge and Au-M edge, respectively. In addition, to absorb calibration uncertainties in the responses, we included 2% systematic errors in the individual bins of the XIS and the HXD.

3.2 Analysis of the Hard X-ray Spectrum

Below, the time-averaged Suzaku spectra are analyzed in detail. We first focused on the HXD data, to study the spectral profile in the hard X-ray band above 10 keV. The time-averaged HXD (PIN+GSO) spectrum spanning 15–168 keV was reproduced well by a power-law model with a photon index of $\Gamma = 2.0 \pm 0.4$, which gave a reduced chi-squared of $\chi^2/\text{d.o.f} = 37/44$. The same spectrum was also fitted with the thermal Comptonization model `nthcomp` (Zdziarski et al. 1996; Życki et al. 1999), which computes a thermal Comptonization spectrum using the photon

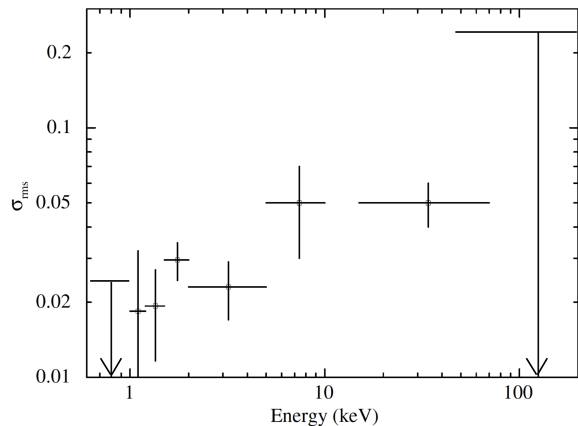


Fig. 4. Energy dependence of the rms variability σ_{rms} obtained from the XIS0, PIN, and GSO light curves in 128 s bins.

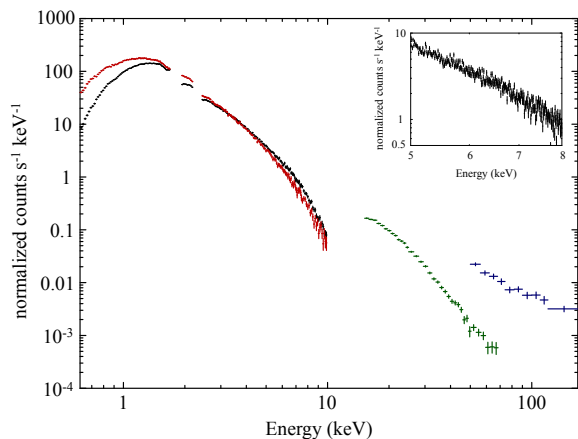


Fig. 5. Time-averaged spectra of MAXI J1828–249 obtained with XIS0 and XIS3 (black), XIS1 (red), PIN (green), and GSO (blue). The inset shows an enlarged view of the XIS0+XIS3 data around the iron $K\alpha$ line energies, obtained without discarding the image core.

index Γ , the electron temperature kT_e , the seed photon temperature kT_{bb} , and the normalization as free parameters. We adopted the disk blackbody as the seed photon source, and set $kT_{\text{bb}} = 0.64$ keV, which was determined by incorporating the XIS data (see Section 3.3.3). This seed-photon temperature, which is well below the energy range of the HXD, does not affect the spectral shape above 10 keV. This model was found to provide an equally good fit ($\chi^2/\text{d.o.f} = 37/43$). The fit gave $\Gamma = 2.0 \pm 0.3$, which agrees with the power-law fit result, and the electron temperature was constrained only poorly as $kT_e > 167$ keV, evidently because of the very flat shape of the hard tail.

3.3 Analysis of the Broadband X-ray Spectrum

We next analyzed the XIS and HXD spectra jointly. The cross-normalizations of PIN and GSO with respect to FI-XISs were

fixed at 1.164³, and that of BI-XIS was left free. When using a convolution model, we extended the energy band to 0.01–1000 keV.

3.3.1 Simple Models

The broad-band Suzaku spectra were fitted jointly with a simple model consisting of a multi-color disk blackbody (`diskbb`; Mitsuda et al. 1984) plus a power-law model. The interstellar absorption was represented by `tbabs` (Wilms et al. 2000). However, when the photon index Γ is varied, it became much higher ($\Gamma \sim 2.5$) than is indicated by the HXD data ($\Gamma = 2.0 \pm 0.4$, subsection 3.2), and the fit failed with $\chi^2/\text{d.o.f} = 843/472$. In particular, The HXD data deviated significantly from the model. This is because the XIS data have much better statistics than the HXD data, and the power-law component favored to fit the structure at the high energy end of the XIS spectrum (see below). We thus fixed Γ at the value of 2.0 determined in subsection 3.2. This model was found to give a very poor fit, with $\chi^2/\text{d.o.f} = 2682/468$. Figure 6 (a) compares the data and the model in this unsuccessful fit, where significant positive residuals remained around 5–10 keV.

This discrepancy could be caused by deformation of the disk emission spectrum due to relativistic effects, which are not considered in the `diskbb` model. We assessed this possibility by replacing the `diskbb` component to the `kerrbb` model (Li et al. 2005), which is a relativistic disk blackbody emission model for an accreting black hole with an arbitrary spin. Its input parameters are the spin parameter, the black hole mass, the inclination angle and distance of the system, the mass accretion rate, the color hardening factor, and another parameter η which expresses the torque at the disk inner boundary. We fixed η at 0 (corresponding to a torque-free inner edge), the distance at 8 kpc, and the hardening factor at 1.7 (Shimura & Takahara 1995), and let the other parameters vary freely. However, as shown in figure 6(b), the residual structure was not substantially mitigated from the `diskbb+powerlaw` ($\Gamma = 2.0$) fit, and the fit ended with $\chi^2/\text{d.o.f} = 1619/472$. Therefore, an additional spectral component is likely to be present at 5–10 keV.

3.3.2 Single-Zone Comptonized Corona with Reflection

An alternative explanation of the structure in 5–10 keV is a broad Fe- $K\alpha$ emission line produced when the Comptonized photons are reflected on the disk (e.g., Reis et al. 2010). The emission line can be strongly broadened due to the relativistic effects, if the reflected photons come from a close vicinity of the black hole. To test if this is the case, we next added a relativistic reflection component to the `diskbb` plus power-law model. Specifically, we adopted `ireflect` and `kdblur` as the reflection model and its relativistic smearing, respectively.

³ <http://www.astro.isas.ac.jp/suzaku/doc/suzakumemo/suzakumemo-2008-06.pdf>

The `ireflect` model, which is a convolution version of the `pexriv` model (Magdziarz & Zdziarski 1995), calculates a reflection spectrum generated by ionized materials. Its free parameters are; the solid angle Ω of the reflector normalized by 2π , which parametrizes the reflection strength; the ionization parameter defined as $\xi = L_X/(nR^2)$, where L_X , n , and R are the ionizing luminosity in 0.005–20 keV, the density of the reflector, and the distance from the X-ray source; and the temperature of the reflector, T_{disk} . The reflector was assumed to have solar abundances, and T_{disk} was fixed at 30000 K because it cannot be constrained by the Suzaku data. Because the `ireflect` model does not account for any emission lines, we added a Gaussian component as the Fe-K α emission line. The normalization of Gaussian was linked with $\Omega/2\pi$ of `ireflect`, so that the line equivalent width with respect to the reflection continuum is always kept to be ~ 1 keV, a typical value for reflection in black hole accretion disks (Matt et al. 1991). To reproduce the strong residual structure in 5–10 keV, we tested the case of $\Omega/2\pi = 2$, in which the reflector covers the entire solid angle. As the data favored high ionization as $\xi \sim 10^4$ erg cm s $^{-1}$, we fixed the line-center energy at 6.9 keV, to make it is consistent with the ξ value.

The `kdblur` model (Laor 1991) is a convolution model to smear, by relativistic effects, a spectrum generated in the inner part of accretion disks. It has four input parameters: the inner and outer radii of the accretion disk (R_{in} and R_{out} , respectively) in units of GM_{BH}/c^2 , where G , M_{BH} , and c are the gravitational constant, the black hole mass, and the light speed, respectively; the inclination angle i ; and the emissivity index β , which dictates that the line emissivity scales as $\propto R^{-\beta}$. Together with $i = 60^\circ$ and $R_{\text{out}} = 400R_g$, we assumed $\beta = 3$, which is expected in a flat disk illuminated by a point source located in a finite distance above the black hole. To investigate the case wherein the reflection spectrum is maximally smeared, we fixed $R_{\text{in}} = 1.235$, which implies an extreme Kerr black hole.

Combining all the components described above, we constructed a model expressed as `tbabs*(diskbb+kdblur*(gauss+ireflect*powerlaw))`, and applied it to the data. However, as shown in figure 6(c) the model failed to explain the observed structure in 5–10 keV, and the reflection continuum overestimated the X-ray flux around 20 keV. Thus, the obtained fit statistics, $\chi^2/\text{d.o.f} = 3988/472$, became much worse than those obtained with the simpler models tested above.

3.3.3 Double Comptonization Model

Yet another possibility is that the observed structure is an additional Comptonization component, on top of the main power-law tail which dominates the hard X-ray flux above 10 keV. Indeed, in some previous works of BHs in the high/soft state, and the intermediate state with a strong disk black-

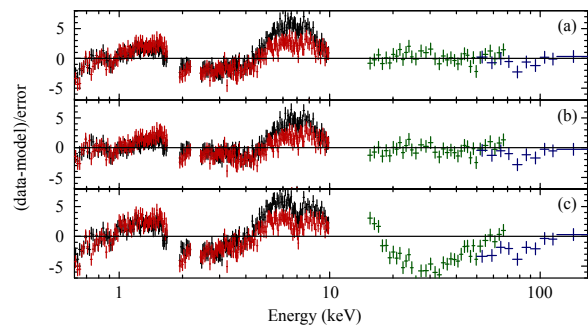


Fig. 6. (a–c) Ratios between the data and the individual models, using the same colors as in figure reffig:fig3: (a) `tbabs*(diskbb+powerlaw)`, (b) `tbabs*(kerrbb+powerlaw)`, and (c) `tbabs*(diskbb+kdblur*(gauss+ireflect*powerlaw))`.

body component which is called the “soft intermediate state”, the X-ray spectra were successfully reproduced by two different Comptonization components (e.g., Kubota et al. 2001; Kolehmainen et al. 2011; Nakahira et al. 2012; Kawano et al. 2017). We adopted this “double Comptonization” model in an attempt to describe the residual structure in 5–10 keV, and considered two different geometries of the plasma responsible for this additional Comptonization: (1) it fully covers the standard disk (e.g., Nakahira et al. 2012), and (2) it covers the disk only partially, and the remaining part of the disk is directly visible (e.g., Kawano et al. 2017).

To test the case (1), we replaced, following Nakahira et al. (2012), the direct MCD component in the MCD+power-law model to the Comptonization component `compPS` (Poutanen & Svensson 1996). Using the numerical solutions of the radiative transfer equation, the `compPS` model produces the Comptonized spectrum, in terms of the electron temperature, the optical depth τ of scattering, the energy distributions of incident photons and electrons, and geometry of the electron cloud. We assumed the MCD emission as the seed photons, chose the “slab” geometry (`geom = 1`) for the electron cloud, and considered only thermal electrons (`gmin = 1`). In this case, the normalization of `compPS` is defined as that of the seed spectrum (i.e., the disk blackbody spectrum), in the same way as `diskbb`. This model can reproduce the reflection component, but we ignored it here by setting the solid angle of the reflector as $\Omega = 0$.

The `compPS+powerlaw` model has successfully reproduced the spectrum, with $\chi^2/\text{d.o.f} = 452/464$ which is greatly improved over the MJD+power-law model. The best-fit parameters and the fit results are presented in figure 7a and table 1, respectively. Thus, the residual feature in 5–10 keV has disappeared. The `compPS` parameters became $kT_e = 14 \pm 7$ keV, which is relatively low, and $\tau = 1.0^{+1.1}_{-0.4}$.

Next, to test the case (2), we added an `nthcomp` model to the MCD+power-law model, following Kawano et al. (2017), and constructed a model as `tbabs*(diskbb+powerlaw+nthcomp)`. The reason for using `nthcomp`, instead of `compPS`, is that

`nthcomp` is suited to cases with $\tau \gtrsim 2$ and relatively low kT_e (Życki et al. 1999), compared to `compPS` which is appropriate for cases with $\tau \lesssim 1$ and high kT_e . The choice is justified later by the fit result. Again, the MCD spectrum was assumed as the seed spectrum for `nthcomp`, and its innermost temperature was linked to that of the main MCD component. As shown in figure 7(b) and table 1, this model has also given an acceptable fit, with $\chi^2/\text{d.o.f} = 440/463$, which is comparable to that of the `compPS+powerlaw` fit. To fit the structure at 5–10 keV, the `nthcomp` model attained a low temperature as $kT_e = 1.2^{+0.3}_{-0.05}$ keV, and a photon index of $\Gamma = 1.0^{+2.6}_{-1.0}$ pegged. The optical depth of the Comptonized cloud was estimated as > 3.5 , from Γ and kT_e of the best-fit `nthcomp` model, assuming a slab geometry, and using the equation in Zdziarski et al. (1996) and Hori et al. (2014), as

$$\tau = \frac{1}{2} \left[\sqrt{\frac{9}{4} + \frac{3}{\frac{kT_e}{mc^2} \left(\left(\Gamma + \frac{1}{2} \right)^2 - \frac{9}{4} \right)}} - \frac{3}{2} \right]. \quad (2)$$

Therefore, the use of `nthcomp` has been justified. This implies a much lower kT_e and a much higher τ , compared with the case (1) solution.

Based on the above two models, we also calculated the inner radius R_{in} of the standard disk, considering both the direct disk photons and the Compton-scattered photons. Assuming the conservation of the number of disk photons, there holds a relation as

$$\frac{F_{\text{disk}}^{\text{P}}}{2 \cos i} + F_{\text{thc}}^{\text{P}} = 0.0083 \left[\frac{R_{\text{in}}}{(D/10 \text{ kpc})^2} \right] \left(\frac{T_{\text{in}}}{1 \text{ keV}} \right)^3 \text{ photons s}^{-1} \text{ cm}^{-2}, \quad (3)$$

where $F_{\text{disk}}^{\text{P}}$ and $F_{\text{thc}}^{\text{P}}$ represent the 0.01–100 keV photon flux in the observer’s direction of the disk component and that of isotropic Comptonization components, respectively (Kubota & Makishima 2004). This equation assumes that $F_{\text{disk}}^{\text{P}}$, namely, the disk flux emitted towards the observer, has an intrinsic emissivity which is proportional to $\cos i$, and the denominator $2 \cos i$ is meant to correct the observed $F_{\text{disk}}^{\text{P}}$ for this implicit effect. As a result, the equation becomes rather inaccurate towards $i \rightarrow 90^\circ$. The factor of 2 is introduced simply because $2 \cos i$ becomes unity when we take its spherical average. The Comptonized photons are assumed to have rather weak anisotropy, if any. Furthermore, this equation assumes that few photons are scattered back to the disk, so that the corona-to-disk feedback effects are negligible. This condition is satisfied if the corona has a low optical depth. It is considered to apply to the present case, wherein $F_{\text{thc}}^{\text{P}}$ is dominated by the $\Gamma = 2$ power-law, of which the source corona is likely to have a rather low optical depth from Equation (2), $\tau < 0.4$, assuming a thermal Comptonization origin with $kT_e > 169$ keV.

Our best-fit case (2) model gave $F_{\text{disk}}^{\text{P}} = 11.1 \text{ photon s}^{-1} \text{ cm}^{-2}$ and $F_{\text{thc}}^{\text{P}} = 37.1 \text{ photon s}^{-1} \text{ cm}^{-2}$, which yield $R_{\text{in}} =$

$(1.2 \pm 0.2) \times 10^2 (\cos i / \cos 60^\circ)^{-1/2} (D/8 \text{ kpc}) \text{ km}$. By multiplying the correction factor 1.19 (e.g., Kubota et al. 1998; Shidatsu et al. 2011), which is based on the color hardening factor 1.7 (Shimura & Takahara 1995) and the stress-free inner boundary condition, the actual inner disk radius is estimated as $R_{\text{in}}^* = (1.4 \pm 0.1) \times 10^2 (\cos i / \cos 60^\circ)^{-1/2} (D/8 \text{ kpc}) \text{ km}$. In the case (1) model, we estimated $F_{\text{thc}}^{\text{P}} = 36.4 \text{ photon s}^{-1} \text{ cm}^{-2}$ from the power-law component, and $F_{\text{disk}}^{\text{P}} = 11.6$ from the seed spectrum of the `compPS` component, which was obtained by using `diskbb` with its normalization set to the best-fit normalization of `compPS`. These values gave, after multiplying the correction factor, 1.19, $R_{\text{in}} = (1.5 \pm 0.1) \times 10^2 (\cos i / \cos 60^\circ)^{-1/2} (D/8 \text{ kpc}) \text{ km}$, which is consistent with that obtained from the case (1) modeling. However, these values are still subject to various systematic uncertainties, because there can be other possible model variants besides the two cases considered here.

3.4 Search for Ionized Absorption Lines

The XIS spectra were searched for highly ionized absorption lines, originating e.g., from disk winds. To improve the photon statistics, we used the data extracted from the whole $108''$ circular region in the XIS image, without excluding the PSF core. However, as shown in the inset of figure 5, no absorption lines were found around the energies of the Fe K lines. To determine the upper limits on the H-like and He-like Fe lines at 6.7 keV and 6.9 keV, respectively, which are usually the strongest lines in other BHBs with winds, we fitted the whole-region XIS spectrum again with the `diskbb+nthcomp+powerlaw` model, plus two Gaussians representing the two lines. We fixed the line center energies of the Gaussians at 6.7 keV and 6.9 keV, and the line widths at 10 eV, which is much smaller than the energy resolution of the XIS. In addition to the two Gaussian normalizations which are assumed to be negative, we varied the normalizations of the continuum components and the photon index of `powerlaw`, but fixed the other continuum parameters at the best-fit values obtained in section 3.3.3. From this analysis, the upper limits of the equivalent widths of H-like and He-like Fe lines were estimated to be 10 eV and 9 eV, respectively. These values are not expected to differ significantly, even if the lines are Doppler shifted as observed in some other BHBs (e.g., Miller et al. 2006; Ueda et al. 2009).

4 Optical Observations and Results

4.1 Observation and Data Reduction

As indicated in figure 5, optical photometric observations of MAXI J1828–249 in the *R* and *I* bands were carried out on 2013 October 21 UT 9:25, simultaneously with the Suzaku observation. We used Hiroshima One-shot Wide field Polarimeter (HOWPol; Kawabata et al. 2008), attached to the Kanata

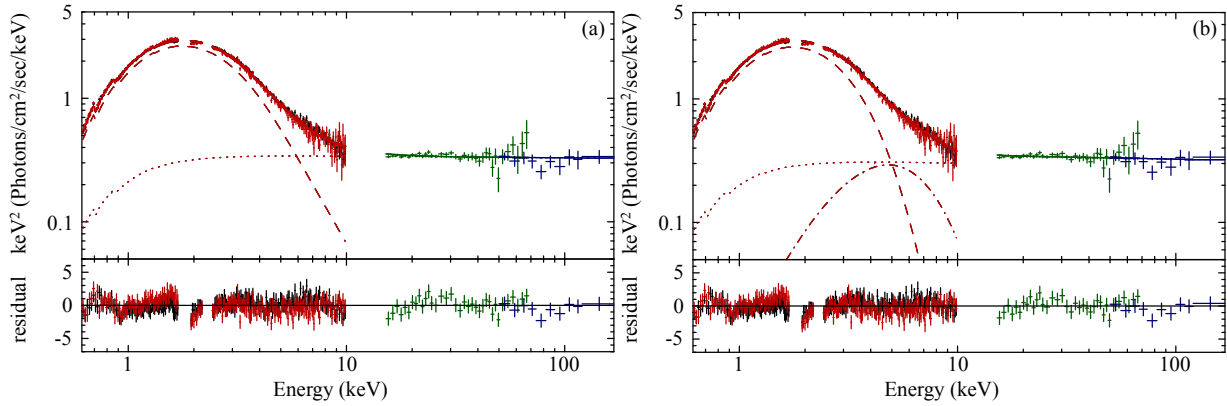


Fig. 7. Time-averaged Suzaku spectra of MAXI J1828–249, fitted with two successful double-Comptonization models, using the same colors as in figure 5. (a) The fit with the `tbabs*(compPS+powerlaw)` model, i.e., the case (1) modeling, where the dashed and dotted lines indicate the `compPS` and `powerlaw` components, respectively. (b) The fit with the `tbabs*(diskbb+nthcomp+powerlaw)` model, i.e., the case (2) modeling, where the dashed, dot-dashed, and dotted lines indicate the `diskbb`, `nthcomp`, and `powerlaw` components, respectively. The lower panels show residuals between the data and the model.

Table 1. Best-fit parameters of the finally accepted two double-Comptonization models.

Component	Parameter	Case (1) model*	Case (2) model†
<code>tbabs</code>	$N_{\text{H}} (10^{22} \text{ cm}^{-2})$	0.201 ± 0.005	0.194 ± 0.004
<code>diskbb</code> ‡	$kT_{\text{in}} (\text{keV})$	-	$0.642^{+0.006}_{-0.025}$
	norm	-	$(2.6 \pm 0.1) \times 10^3$
<code>compPS</code> , <code>nthcomp</code> §	$kT_{\text{bb}} (\text{keV})$	$0.60^{+0.02}_{-0.01}$	$= kT_{\text{in}}$
	$kT_{\text{e}} (\text{keV})$	14 ± 7	$1.2^{+0.3}_{-0.1}$
	Γ_{th}	-	$1.0^{+2.6}_{-1.0}$ pegged
	τ	$1.0^{+1.1}_{-0.4}$	$> 3.5^{\parallel}$
	norm	$(3.4 \pm 0.3) \times 10^3$	$1.4^{+17.8}_{-0.1} \times 10^{-2}$
<code>powerlaw</code>	Γ	2.01 ± 0.04	2.03 ± 0.03
	norm	0.35 ± 0.05	$0.33^{+0.04}_{-0.03}$
	χ^2/dof	451.69/464	440/463

The `tbabs(compPS+powerlaw)` model, which assumes all disk photons are Comptonized into the `compPS` component.

†The `tbabs*(diskbb+nthcomp+powerlaw)` model, which assumes that only a fraction of disk photons are Comptonized, as represented by `nthcomp`.

‡Not used in the case (1) model.

§The seed spectrum was assumed as an MCD (i.e., `inp_type` was set to 1 for `nthcomp` and the seed temperature to a negative value for `compPS` in XSPEC). The seed temperature kT_{bb} was linked to kT_{in} of the `diskbb` component in the case (2) model.

|| Calculated through Equation (2).

1.5 m telescope at Higashi-Hiroshima Observatory, Hiroshima Astrophysical Science Center, Hiroshima University. On that night, $60 \text{ s} \times 9$ *I*-band exposures were taken, followed by $60 \text{ s} \times 66$ *R*-band exposures.

Using IRAF⁴, we reduced the data in a standard way for optical imaging observations; bias subtraction and flat fielding were applied to the individual frames. The apparent magnitude of the target in each frame was estimated via PSF photometry, using 6 reference stars near the target in the field of view. The magnitude error in each frame was calculated as standard deviation of the relative magnitudes derived using different reference stars. The apparent magnitudes in the *R* and *I* bands, averaged over the entire observation periods, were ≈ 17 mag and ≈ 16 mag,

⁴ <http://iraf.noao.edu/>

respectively, in the Vega unit.

We also used the optical and UV data (OBSID=00032997006) of the Swift UltraViolet and Optical Telescope (UVOT; Roming et al. 2005) obtained on the same day, but ~ 1 hour before the start of the Suzaku observation. Specifically, the UVOT observation was performed from 2013 October 21 UT 04:25 to 04:42 through *UVW1*, *U*, *B*, *UVW2*, *V*, and *UVM2* filters, with a net exposure of 85–342 s each. We defined the source area as a circle of a $5''$ radius, centered at the source position, and derived the source fluxes in the individual bands with a `ftool uvot2pha`. The background levels were estimated from source-free regions.

In addition to the above observations in the outburst, we searched archival data in quiescent phases for possible detec-

tions of the optical counterpart of MAXI J1828–249. The source was detected in the Pan-STARRS (Panoramic Survey Telescope and Rapid Response System) project in the g , r , i , z and y bands, on 2012 August 25. The i and r -band apparent magnitudes were 18 and 19 (in the AB magnitude unit), respectively. When converted to the flux unit, these values imply that the object was about 4 times fainter than in our Kanata observations.

4.2 Analysis of the Multi-Wavelength Spectral Energy Distribution

Figure 8 presents the quasi-simultaneous multi-wavelength spectral energy distribution (SED) of MAXI J1828–249, produced from the time-averaged data of Suzaku, Kanata, and Swift/UVOT. It is corrected for the X-ray absorption and the optical/UV extinction, using the model described below. The Pan-STARRS data are also shown in the same figure. Using these data, we investigated the origin of the optical/UV emission.

While the X-ray emission from BHBs is most likely generated in the inner region of the accretion flow, their optical photons are considered to originate potentially from multiple sources, including synchrotron emission from jets, thermal emission from the outer disk region, and blackbody emission from the companion star. In the present case, the jet emission is unlikely to contribute to the optical flux, because normally jets are not observed when the X-ray spectrum is dominated by the MCD emission (Fender 2001; Fender et al. 2001; Fender et al. 2004a; Fender et al. 2004b). Indeed, the source was not detected in the radio observation performed 3 days before our Suzaku observation (Miller-Jones et al. 2013), whereas detected after the source returned to a genuine low/hard state (Corbel et al. 2014), which took place ~ 4 months later. The emission from the companion star is also unlikely to be a main contributor to the optical flux. In fact, the Pan-STARRS data taken before the outburst indicate that it contributes only up to $\sim 20\%$ of the optical flux (figure 8). Hence, we infer that the optical emission of MAXI J1828–249 in the outburst was predominantly produced in the outer disk as thermal emission.

To confirm the above inference and investigate the outer disk conditions, we analyzed the quasi-simultaneous multi-wavelength SED obtained with Suzaku, Kanata, and Swift/UVOT, using a broad-band continuum SED model consisting of the disk emission and its Comptonization. Normally, the outer disk emission of BHBs is significantly enhanced due to irradiation by the X-rays from the inner disk region (e.g., Gierliski et al. 2008, 2009), and thus the optical and UV fluxes exceed the lower-frequency extrapolation of the X-ray-determined MCD component. To take into account this effect, we adopted `optxrpilr` model (Shidatsu et al. 2016, Kimura &

Table 2. Best-fit parameters of the `optxrpilr` model.

Component	Parameter	Value
redden	$E(B - V)^*$	0.246 ± 0.005
tbabs	N_{H} (10^{22} cm $^{-2}$)	0.142 ± 0.003
optxrpilr	M_{BH} (M_{\odot})	4.0 (fixed)
	D (Mpc)	0.008 (fixed)
	$\log(L/L_{\text{Edd}})$	-0.840 ± 0.002
	a_{star}	0 (fixed)
	R_{cor} (R_{g})	44 ± 2
	$\log R_{\text{out}}$ (R_{g})	5.3 ± 0.1
	τ	6.0 ± 0.6
	R_{pl} (R_{g})	$14.30^{+0.09}_{-0.08}$
	Γ_{h}	2.0 (fixed)
	kT_{eh} (keV)	1000 (fixed)
	f_{out}	$(3.2^{+0.9}_{-0.8}) \times 10^{-4}$
	albedo	0.3 (fixed)
	norm	1.0 (fixed)
	χ^2/dof	539/472

* $E(B - V)$ is set to be $N_{\text{H}}/(5.8 \times 10^{21}$ cm $^{-2}$).

Done 2018) to fit the SED.

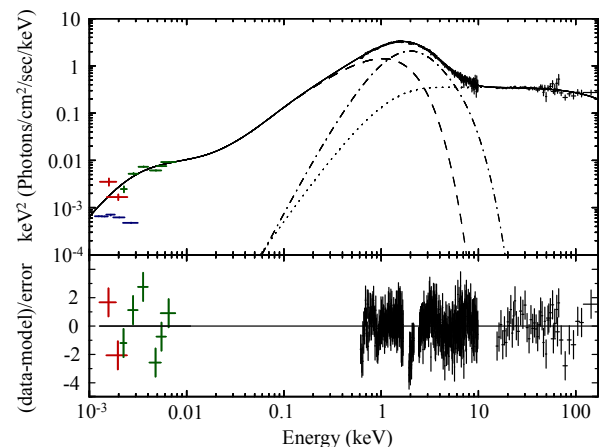


Fig. 8. Multi-wavelength SED of MAXI J1828–249, obtained with Suzaku (black), Kanata (red), and the Swift/UVOT (green), fitted with the `optxrpilr` model (black solid line). The Pan-STARRS data taken on 2012 August 25 (before the outburst; not used in the SED fit

) are also plotted in blue. The data and model are corrected for the interstellar absorption and extinction. The dot-dashed, dotted, and dashed lines indicate the contribution of the soft and hard Comptonization components, and the direct disk emission including the reprocessed component, respectively. The bottom panel shows the residuals between the data and the best-fit model.

The `optxrpilr` model calculates a disk-emission spectrum and its Comptonization components, considering the irradiation of outer disk regions by the X-rays from the inner disk region. Like the predecessor SED models `optxagnf` (Done et al. 2012) and `optxirr` (Sutton et al. 2014), it includes two different Comptonization components: a power-law tail computed based on the `nthcomp` code (Zdziarski et al. 1996; Życki

et al. 1999) using the photon index Γ_h and an electron temperature kT_{eh} as free parameters, and a low-temperature thermal Comptonization component, which is based on the `compTT` code (Titarchuk & Lev 1994) and is parametrized by the optical depth τ and another electron temperature kT_{es} . The former is meant for the power-law tail generally seen in the high/soft state, and the latter for an additional lower-temperature Comptonization component, like the one which we found in the Suzaku spectrum. Here we set $kT_{eh} = 1000$ keV, because no significant exponential cutoff is present in the Suzaku energy band (figure 7b), and fixed $\Gamma_h = 2.0$, as obtained in section 3.3.3. This model considers X-ray reprocessing effect, whose strength is determined by the height-to-radius ratio f_{out} of the outer disk, and the albedo a_{out} . Because it is difficult to constrain the two parameters simultaneously, we fixed a_{out} at 0.3, following Shidatsu et al. (2016), and allowed f_{out} to vary. Further details of this model are given in Appendix 1.

The interstellar X-ray absorption and the optical/UV extinction were expressed by the `tbabs` and `redden` models, respectively. The `redden` model calculates interstellar extinction with the reddening factor $E(B - V)$ as an input parameter, assuming the extinction factor $R_V = A_V/E(B - V) = 3.1$, where A_V is the extinction measured in the V band. We varied N_H of `tbabs` and linked it to $E(B - V)$ of `redden`, so that they always satisfy the relation obtained by Bohlin et al. (1978), $N_H/E(B - V) = 5.8 \times 10^{21} \text{ cm}^{-2} \text{ mag}^{-1}$.

This model was found to give an acceptable fit to the wide-band SED, with $\chi^2/\text{d.o.f} = 539/472$. The derived best-fit model is shown in figure 8, and its parameters are listed in table 2. The irradiation strength, i.e., the fraction of X-rays reprocessed by the outer disk was obtained as $F_{out} = (1 - a_{out})f_{out} = (2.3^{+0.5}_{-0.6}) \times 10^{-4}$. Because this is securely positive, the X-ray reprocessing effect is considered to have been significant in the outburst. Indeed, as shown in figure 8, the optical and UV fluxes, corresponding to the outer disk emission, is strongly enhanced over the simple MCD extrapolations which would have a constant logarithmic slope toward lower energies.

In figure 8, the MCD component and the soft Comptonization component add up to the soft X-ray spectrum in somewhat different ways than was obtained in subsection 3.3.3. This is mainly due to the difference of the modeling of the hard Comptonization component; the X-ray data analysis employed a power-law model which extends towards lower energies, whereas the SED analysis utilized `nthcomp` which drops off below the seed photon peak. However, the parameters related to the irradiation of the outer disk, f_{out} and R_{out} (see Appendix 1), which are the most important parameters in this SED analysis, are not significantly affected by this difference, because they are determined by the bolometric flux.

5 Discussion

5.1 Summary of the Results

Using Suzaku, we observed MAXI J1828–249 on 2013 October 21–22, and have successfully obtained broad-band X-ray data. It was ~ 6 days after the MAXI discovery and the start of the spectral softening, and the source was in the brightest and softest condition ever achieved in the 2013 outburst. Analyzing the Suzaku data, we have obtained the following results.

1. The rms variability of the 128-s binned light curve is 2–3% in 0.6–5 keV (XIS), $\sim 5\%$ in 5–10 keV (XIS) and 15–70 keV (HXD-PIN), and $< 24\%$ in 50–200 keV (HXD-GSO).
2. No absorption lines are seen around the Fe-K energy region, beyond an upper limit of ~ 10 eV in equivalent width.
3. The 0.6–168 keV spectrum consists of a soft component, and a clear hard-tail component which extends at least to ~ 170 keV with $\Gamma \sim 2.0 \pm 0.4$ without bending. The Comptonization modeling of the hard tail yields $kT_e > 167$ keV.
4. Although the continuum shape is typical of BHBs, positive excess remains in 5–10 keV when the spectrum is fitted with a simple MCD+power-law model. The residuals cannot be explained either by relativistic broadening of the disk emission, or by relativistic reflection which includes a broad Fe-K line.
5. The spectrum can be instead reproduced successfully by adding a softer thermal Comptonization component, assuming seed-photon supply from the disk. The Comptonizing electron cloud covers the disk either entirely with $kT_e \sim 14$ keV and $\tau \sim 1$, or partially with $kT_e \sim 1.2$ keV and $\tau > 3.5$.
6. Regardless of the above ambiguity in the soft Compton cloud, the innermost radius of the accretion disk is estimated as $R_{in} \sim 1.5 \times 10^2 (\cos i / \cos 60^\circ)^{-1/2} (D/8 \text{ kpc}) \text{ km}$.

Combining the present X-ray and optical data, with the two radio results (subsection 2.1), and the archival optical data in an X-ray quiescence, we have found that the optical emission of MAXI J1828–249 in our observations is likely to have been dominated by the irradiated outer disk emission, rather than the companion star or the jet emission. In fact, the multi-wavelength SED in the outburst was successfully described by a model consisting of the irradiated accretion disk emission and its Comptonization components.

5.2 Identification of the Spectral State

To identify the spectral state of MAXI J1828–249 in the Suzaku observation, we compare in table 3 its characteristic parameters with those typically seen in the high/soft state and low/hard state. The overall shape of the broad-band spectrum, the inner disk temperature of ~ 0.6 keV, and the power-law ($\Gamma \sim 2$) shaped hard tail without exponential cutoff, are all

consistent with those of BHBs in the normal high/soft state. However, the intensity of the hard tail, relative to that of the MCD component, is somewhat large compared with what is usually seen in the high/soft state. In fact, as shown in figure 7a, the hard tail of MAXI J1828–249 is only ~ 6 times fainter in the EF_E form than the soft X-ray peak, whereas typical high/soft-state spectra have the hard tails which are >10 times fainter than their peaks (e.g., Done et al. 2007). Similarly strong hard tails are seen in other transient BHBs, such as GX 339–4 (e.g., Kolehmainen et al. 2011; Plant et al. 2014), Swift J1753.5–0127 (Chiang et al. 2010) and MAXI J1910–057 (Nakahira et al. 2014), mainly during their state transitions. In reference to these knowledges accumulated so far, the present case of MAXI J1828–249, of which the power-law component contributes $\sim 40\%$ of the 2–15 keV flux, may be classified as soft intermediate state (Homan & Belloni 2005; Plant et al. 2014).

The soft Comptonization component, which is responsible for the 5–10 keV excess, could be taken as another evidence for the intermediate state. Actually, a similar soft Comptonization component is often seen in Cygnus X-1, and it becomes enhanced in the intermediate state (Yamada et al. 2013; Kawano et al. 2017). Similar examples include GX 339–4 (Tamura et al. 2012) and XTE J1550–564 (Gierlinski & Done 2003). However, this intermediate component is also observed in the high/soft state of some BHBs (Kolehmainen et al. 2011; Shaw et al. 2016). Therefore, it may be a preferred but not definitive feature of the intermediate state (see also subsection 5.3).

In addition to the spectral properties, the source has somewhat stronger variability, on time scales of 128 s to several tens ks, than transient BHBs in the high/soft state (table 3). Specifically, the estimated rms variability of MAXI J1828–249 in 5–10 keV, $\sim 5\%$, is larger than those in the typical high/soft state below ~ 10 keV, $\sim 1\%$ (Heil et al. 2015), but comparable to those of the intermediate state (e.g., Hori et al. 2014). Further discussion continues in subsection 5.3.

Another interesting property of MAXI J1828–249 is its behavior on the hardness intensity diagram through the outburst, where no significant hysteresis is seen. This is reminiscent of that of MAXI J1836–194, which exhibited an incomplete state transition and never reached the high/soft state. Considering all the above results, and presuming that the hysteresis is observed only after the source completed its hard-to-soft state transition, we infer that MAXI J1828–249 stayed in the soft intermediate state and did not reach the genuine high/soft state in the Suzaku observation, as also suggested by Filippova et al. (2014). The observed properties of MAXI J1828–249, including the strong hard tail and relatively enhanced variability above ~ 5 keV, are literally between those in the low/hard state and the high/soft state (table 3). The soft intermediate state seems to be fairly stable at least in this object, as the hardness ratio stayed almost

constant for ~ 20 days around the Suzaku observation.

5.3 Nature of the Additional Intermediate Component

Here, we investigate the nature of the additional spectral structure found in 5–10 keV. This is considered to be a relatively stable feature of MAXI J1828–249, as it is also present in the simultaneous Swift and INTEGRAL spectra (Grebenev et al. 2016), taken on October 15–18 which are several days before our Suzaku observation. This component is likely to be mildly variable, because the rms variability in 5–10 keV ($\sim 5\%$) is larger than that in 0.6–5 keV where the raw disk emission is seen (figure 6), and is comparable to that in 15–70 keV where the hard tail dominates. Although the varying hard tail would add to the 5–10 keV variability, this can explain the observed 5–10 keV variability at most only partially, because the hard-tail photons contribute only $\sim 50\%$ in this energy band.

The 5–10 keV structure in the Suzaku data has been reproduced equally well by the two variants of Comptonization. One (case 1) assumes that the entire disk region emitting X-rays is covered by a relatively thin ($\tau \sim 1$) Comptonizing electron cloud with $kT_e = 14 \pm 7$ keV, so that the original MCD emission as a whole is modified into a Comptonized spectrum with a higher color temperature. The other (case 2) is a condition wherein a thick ($\tau > 3.5$) and much cooler ($kT_e \sim 1.2$ keV) Compton cloud covers a part of the disk, and the produced Wien hump peaked at $4kT_e \sim 5$ keV is added to the direct MCD emission.

The above two alternative solutions can be distinguished by a parameter $Q \equiv T_e/T_{\text{in}}$. First introduced by Makishima (2014) and applied to various classes of accreting X-ray sources (Zhang et al. 2016; Kobayashi et al. 2017), it serves as a good indicator of the balance between Compton cooling and ionic heating of the electrons. The case 2 modeling yields $Q = 2$, which means that the electrons are strongly cooled to form a “cool and thick” Compton cloud. Such low values as $Q < 7$ are often found also with the Comptonized blackbody radiation of neutron-star low-mass X-ray binaries in their high/soft state (Zhang et al. 2016; Makishima 2014). If adopting the case 1 modeling instead, we obtain $Q = 30$, which is comparable to the values of $Q \sim 50$ found in so-called very high state and hard intermediate state of BHBs (Tamura et al. 2012; Hori et al. 2014). Even higher values as $Q = 10^2 - 10^3$, to be called “hot and thin” Comptonization, are obtained from the hard X-ray continuum of BHBs in the low/hard state (Makishima et al. 2008). Thus, the soft Compton component detected from MAXI J1828–249 is more strongly cooled than the hot inner accretion flows in the low/hard state where the Comptonized hard continuum is produced, and becomes comparable to those in the very high state (case 1 modeling), or even further to reach a “cool and thick” condition (case 2 modeling).

Table 3. Characteristic parameters of MAXI J1828–249 and of BHBs in the typical high/soft and low/hard states*.

Source	general	MAXI J1828–249	general
State	high/soft state	soft intermediate	low/hard state
Disk component			
$F_{\text{disk}}/F_{\text{total}}$ (2–20 keV)	> 0.75	0.63	< 0.2
kT_{in} [keV]	0.6–1.5	0.59–0.65	< 0.7
Hard tail			
$F_{\text{pl}}/F_{\text{total}}$ (2–20 keV)	< 0.25	0.37	> 0.8
Γ	> 2.1	2.0–2.1	1.5–2.0
Exponential cutoff	no	no	yes (at ~ 100 keV)
Variability [†]	$\sim 0.01^{\ddagger}$	$\sim 0.05^{\S}$	$\sim 0.1^{\ddagger}$
Compact jets	no	no	yes

*Mainly taken from McClintock & Remillard (2006) and this work, unless otherwise specified.

[†]Fractional rms variation in a frequency range of 5×10^{-5} – 8×10^{-3} Hz.

[‡]In 2.5–13 keV, calculated by extrapolating the power spectra in 0.04–100 Hz given by Heil et al. (2015).

[§]In 5–10 keV.

So far, cool Comptonization components, similar to the present one, have also been observed from some other BHBs, such as XTE J1752–223 (Nakahira et al. 2012), Cygnus X-1 (Kawano et al. 2017), and GX 339–4 (Kolehmainen et al. 2011), when they showed disk dominant spectra. Therefore, this is neither specific to MAXI J1828–249, nor a rare phenomenon. Nevertheless, the origin of these soft Compton X-rays is still unclear, and leaves us with at least two alternatives corresponding to the case (1)/(2) ambiguity. If adopting the case (2) standpoint, a likely scenario is that the standard disk is still developing toward the ISCO, and the thick and cool Compton cloud is formed in a region where the disk inner edge intrudes into the hot inner flow (e.g., Kawano et al. 2017). Alternatively, we had better employ the case (1) scenario, when the low-temperature Compton component co-exists with a standard disk that is likely to extend down to the ISCO (Kolehmainen et al. 2011). Then, the color hardening effect may be produced by a Comptonizing layer which somehow develops on the disk surface (Kolehmainen et al. 2011; Nakahira et al. 2012).

The energy dependent variability in figure 4 may help us to distinguish the case (1)/case (2) degeneracy. In the case (2) modeling (figure 7b), the emission below ~ 5 keV would be dominated by the disk photons, which are expected to vary only $\sim 1\%$ (table 3). In contrast, the case (1) fit (figure 7a) implies that the entire disk spectrum is Comptonized, so that the signals below ~ 5 keV should be still variable as the corona varies in its optical depth and/or the electron temperature. Thus, the case (1) interpretation would be somewhat favored in MAXI J1828–249.

Whatever the origin of the low-temperature Comptonization component in MAXI J1828–249 is, our result suggests that the multi-zone Comptonization is ubiquitous among various states in BHBs, supposing that the hard tail in the disk dominated states is also produced by Comptonization of the disk photons. In fact, Suzaku observations have shown that a double

Comptonization modeling is often required to reproduce BHB spectra in the low/hard state (Makishima et al. 2008; Takahashi et al. 2008; Shidatsu et al. 2011; Yamada et al. 2013), as well as in the very high state (Tamura et al. 2012; Hori et al. 2014). Recent studies of short-term spectral variations above ~ 0.1 Hz in the low/hard state also support the multi-zone Comptonization picture (Axelsson & Done 2018; Mahmoud & Done 2018). Such a view is likely to apply also to Syfert galaxies, of which so-called soft excess component seen in < 2 keV, is considered to arise as a soft Comptonization component (e.g., Noda et al. 2013). In contrast, a single-zone Comptonization with $Q > 7$ and $Q < 7$ are usually sufficient to describe the low/hard state and high/soft state spectra, respectively, of low-mass X-ray binaries involving weakly-magnetized neutron stars (Sakurai et al. 2014). Therefore, a clue to the problem may be obtained through unified studies of these phenomena in various classes of accreting objects.

5.4 Properties of the Hard Tail

Another important result from the present Suzaku observation is the clear detection of the hard tail, which extends from ~ 15 keV to ~ 170 keV with a very constant slope of $\Gamma = 2.0$ (figure 6). As summarized in table 3, this flatness without high-energy bending makes it more similar to the hard-tail component seen in the high/soft state, than to the low/hard state continuum. Furthermore, the fractional rms variability of the hard tail, $\sim 5\%$ which we measured in 15–70 keV, is similar to those of the hard tail in the high/soft state; in fact, the 10–20 keV signals of Cygnus X-1 in the high/soft state are estimated to vary by $\sim 6\%$, as derived by integrating its long-term 10–20 keV power spectrum, obtained with the MAXI/GSC (figure 3 right of Sugimoto et al. 2016), over 10^{-2} Hz to 10^{-5} Hz which matches with figure 3.

In contrast to the above similarities, some dissimilarities are

also noticed when the hard tail of MAXI J1828–249 is examined from several other aspects (see also table 3). These viewpoints include the rather high hard-tail luminosity relative to the disk luminosity, which we used as the primary feature in our state identification in subsection 5.2, and the value of $\Gamma = 2.0$ which indeed falls on the flattest end and the steepest end of the Γ distributions in the high/soft and low/hard states, respectively. These two properties make the present hard tail literally intermediate between those seen in the two major states. We hence speculate that the hard X-ray continuum in the low/hard state and the hard tail component in the high/soft state are related to each other in one way or another. The hard tail observed from MAXI J1828–249 is possibly a transition state, through which the former changes into the latter.

As described in Section 5.3, we consider Comptonization of disk photons in an electron cloud inside or above the disk, as a plausible origin of the hard tail of MAXI J1828–249. The electrons may have a non-thermal distribution or a thermal distribution with a temperature of > 167 keV. Some previous works proposed Comptonization in jets especially in the low/hard state and the hard intermediate state (e.g., Reig et al. 2003; Markoff et al. 2005, Reig & Kylafis 2015). Although this picture could explain the X-ray emission at the very onset of the outburst before the spectral softening, it is unlikely to give a satisfactory explanation of the hard tail seen in the Suzaku observation. In fact, the radio non-detection (Miller-Jones et al. 2013) suggests that the jets already ceased a few days before that epoch. Multi-wavelength studies in various states would be needed to understand how much jets can contribute to the Comptonization components and how its contribution changes during the state transitions.

5.5 Implication from the Multi-wavelength SED

The optical and X-ray SED in the outburst was successfully reproduced with the `optxrplir` model, one of the latest spectral models of an irradiated accretion disk. The outer disk radius was obtained as $R_{\text{out}} = 10^{5.3} R_g$, which is comparable with those in other transient BHBs with relatively short orbital periods (\lesssim a few days), such as MAXI J1305–704 (Shidatsu et al. 2013), MAXI J1910–057 (Nakahira et al. 2014; Degenaar et al. 2014), and GRO J1655–40 (e.g., Shidatsu et al. 2016), but smaller than those with longer orbital periods, such as GRS 1915+105 (e.g., Frank et al. 1992; Done et al. 2004) and V404 Cygni (Kimura et al. 2016). The estimated value, $R_{\text{out}} \sim 5 (M_{\text{BH}}/5M_{\odot})$ lt-sec is comparable to the Roche-lobe radius of ~ 2 lt-sec, expected when a black hole with $5M_{\odot}$ forms a binary with a main-sequence low-mass star of $\sim 0.5M_{\odot}$ which marginally fills its Roche lobe.

The strength of reprocessing, $F_{\text{out}} = f_{\text{out}} * (1 - a_{\text{out}}) \sim 2.3 \times 10^{-4}$, is $\gtrsim 1$ order of magnitude lower than the typical

values in the high/soft and low/hard states (e.g., Gierliski et al. 2009; Chiang et al. 2010; Rahoui et al. 2012; Shidatsu et al. 2013; Nakahira et al. 2014; Shidatsu et al. 2016; Kimura & Done 2018). This value could be even lower when the contribution of the companion star to the optical and UV fluxes is subtracted. What made the small reprocessed fraction is still unclear, but it could be ascribed to a difference in the geometry of the outer disk, and/or the absorption efficiency on the disk surface. Yet another possibility is that the inner disk is fully covered by the cool Compton cloud (case 1 in subsection 3.3), which is relatively optically thin ($\tau \sim 1$) as seen from above but becomes optically thicker towards directions which are grazing to the disk plane. As a result, the emerging soft X-rays (with the Comptonized color) are mildly collimated in the directions perpendicular to the disk, just like the limb darkening effect seen in the Solar photosphere. If this interpretation is correct, the case (1) double Comptonization would be more favored, in agreement with the inference from the variability (subsection 5.3).

5.6 System Parameters of MAXI J1828–249

Considering our X-ray, optical, and UV results, let us estimate basic parameters of this binary system, including the distance D and the black hole mass M_{BH} . The shadowed region in figure 9 indicates the allowed ranges on the D - M_{BH} space, obtained from the condition that R_{in} estimated from the best-fit double Comptonization model (see subsection 3.3.3) is not smaller than the ISCO radius, R_{ISCO} . The solid lines, derived assuming a non-spinning black hole (i.e., $R_{\text{ISCO}} = 6R_g$) with $R_{\text{in}} = R_{\text{ISCO}}$ and an inclination angle of 60° , move downward, if a lower inclination is assumed. If the black hole is spinning rapidly, both the intensity and shape of the spectrum are affected in complex ways by various relativistic effects, including the decrease in R_{ISCO} , light bending, gravitational redshifts, and Doppler beaming (see e.g., Wang et al. 2018). Further investigation using relativistic disk emission models, however, is beyond the scope of this work and we left as a future work.

Figure 9 also plots the D - M_{BH} relations, derived by estimating the Eddington luminosity of the objects from the actually observed luminosities. Even though MAXI J1828–249 may have stayed in the soft intermediate state without reaching the genuine high/soft state, the MAXI/GSC hardness ratio in figure 1c increased significantly over MJD 56619–56640, while the 15–50 keV Swift/BAT intensity remaining rather constant. We therefore accumulated the MAXI/GSC data taken over this period into a single spectrum, and fitted it successfully with a power-law model with a photon index of ~ 2.4 . The obtained 0.1–100 keV flux, $F = 9.3 \times 10^{-9} \text{ erg s}^{-1} \text{ cm}^{-2}$, may be taken as the value when the system fully returned to the low/hard state. The three curves in figure 9 were derived by equating this F with 1%–4% of the Eddington luminosity, as normally

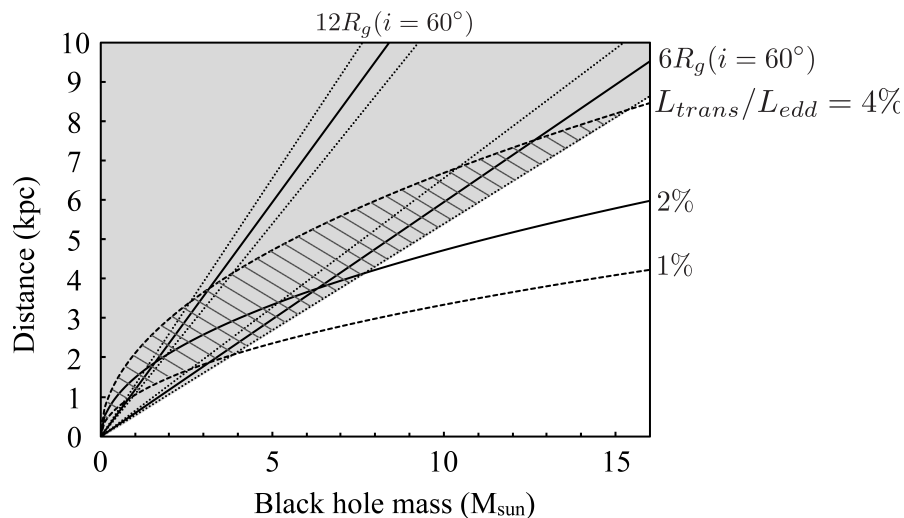


Fig. 9. Constraints on the black hole mass and distance of MAXI J1828–249. Solid lines indicate $R_{\text{in}} = 6R_g$ and $12R_g$, which correspond to R_{ISCO} and $2R_{\text{ISCO}}$, respectively, assuming $i = 60^\circ$ and a non-rotating black hole. Dashed lines show their 90% confidence limits. The shaded region satisfies $R_{\text{in}} \geq R_{\text{ISCO}}$. Solid curves are obtained from the condition that the transition back to the low/hard state took place at 1%, 2%, and 4% of the Eddington luminosity, L_{Edd} . The hatched region satisfies $R_{\text{in}} \geq R_{\text{ISCO}}$ and the soft-to-hard transition luminosity $L_{\text{trans}} = 1\%–4\% L_{\text{Edd}}$.

observed in BHBs (Maccarone 2003). The hatched region indicates where the two different D - M_{BH} relations are satisfied, assuming $i = 60^\circ$.

The exact location of the inner edge of the standard disk is unclear if the source is in the soft intermediate state. Although $R_{\text{in}} \sim R_{\text{ISCO}}$ is a likely condition, previous studies suggest that the standard disk is slightly truncated at less than a few times the ISCO in the very high state (Tamura et al. 2012; Hori et al. 2014). A consistency check of figure 9 may be provided by the N_{H} value of MAXI J1828–249, $(1.5–2.0) \times 10^{21} \text{ cm}^{-2}$, which was obtained by analyzing the X-ray spectrum and the multi-wavelength SED. This is comparable to the total Galactic column, $N_{\text{H}} = 1.6 \times 10^{21} \text{ cm}^{-2}$, and thus the source would be located near the Galactic center or farther. All the available information is consistent with an interpretation that MAXI J1828–249 is a binary consisting of a stellar mass black hole and a low-mass companion, and is located at a distance of several to ~ 7 kpc.

The nature of the companion star is still unknown. Assuming a distance of 8 kpc, the Pan-STARRS data obtained before the outburst yields an absolute V magnitude of $M_V \sim 3$. If the companion star is a main sequence star, it should be an $A \sim F$ -type or later type star (Turon et al. 1992; Turon et al. 1998).

6 Summary and Conclusion

We observed the BHB candidate MAXI J1828–249 in X-ray, UV, and optical bands with Suzaku, Swift/UVOT and Kanata, respectively, when it reached its peak flux in the 2013 outburst. The main conclusions are summarized as follows.

1. The X-ray properties observed with Suzaku, including the somewhat stronger variability and the brighter hard tail than those of typical transient BHBs in the high/soft state, and the non-hysteretic behavior on the hardness intensity diagram, suggest that the source was in the soft intermediate state, rather than the high/soft state.
2. In the X-ray spectrum, a low-temperature Comptonization component is required in addition to the MCD component and the hard tail dominating above ~ 10 keV. This spectral component can be equally well reproduced by assuming that this additional Comptonizing cloud covers the disk either partially or fully. The latter may be favored, considering the energy dependence of the rms variability.
3. The hard tail has transitional properties between those in the typical high/soft state and the continuum in the typical low/hard state. This suggests that they are somehow connected.
4. A dominant fraction of the optical and UV emission was likely to be produced by the outer disk, which is relatively weakly irradiated by X-rays.
5. Constraints on the basic parameters of the binary system, including the black hole mass, distance, and the type of the companion star, were acquired. MAXI J1828–249 is considered as a binary containing a stellar-mass black hole.

Acknowledgments

We are grateful to the Suzaku operation team for carrying out the ToO observation. This research has made use of MAXI data provided by RIKEN, JAXA and the MAXI team. Part of this work was financially supported by Grants-in-Aid for Scientific Research 16K17672 (MS) and

16K05301 (HN) from the Ministry of Education, Culture, Sports, Science and Technology (MEXT) of Japan. MS acknowledges support by the Special Postdoctoral Researchers Program at RIKEN.

Appendix 1 The optxrplir model

Here, we describe the details of the SED model `optxrplir`, utilized in section 4.2. It assumes the Novikov-Thorne emissivity profile (Novikov & Thorne 1973), over the entire region of the accretion disk from the ISCO to the outer disk edge. The ISCO radius is determined by the two input parameters: the black hole mass M_{BH} and the spin parameter a_* , and the outer disk radius is by R_{out} , which specifies the outer disk radius in units of R_{g} . In this model, the direct disk component and the hard and soft Comptonization components which are calculated on the basis of `nthcomp` and `compTT`, respectively, are separated radially; their luminosities are defined as the luminosities of the relativistic standard disk from R_{ISCO} to R_{pl} , R_{pl} to R_{cor} , and R_{cor} to R_{out} , respectively. Thus, the input parameter R_{pl} determines the normalization of the hard Comptonization component, and R_{cor} determines that of the soft Comptonization components. The color-temperature correction is considered for the direct disk spectrum produced in the region above R_{cor} , in the same manner as `optxagnf` (Done et al. 2012). The luminosity of each component is converted to the flux at the observer's position by using the distance D .

To account for the X-ray reprocessing component, `optxrplir` assumes that the disk height $H(r)$ at a radius r is proportional to $r^{9/7}$ and that the illuminating X-ray flux has a radial dependence of $r^{-12/7}$, unlike previous models such as `diskir` (Gierlinski et al. 2008, 2009) and `optxirr`, which assume an r^{-2} dependence for the illuminating flux. The radial dependence adopted in `optxrplir` is based on a theoretical calculation of the irradiated geometrically-thin accretion disk (Cunningham 1976). To determine the strength of the reprocessed component, the `optxrplir` model uses the albedo (a_{out}) and the geometry-dependent factor (f_{out}), as input parameters. The albedo is assumed to be constant radially, and therefore a fraction $(1 - a_{\text{out}})$ of the total incident X-ray flux are reprocessed at each radius. The parameter f_{out} is defined as the ratio of the disk height at the outer edge over the outer radius, and determines the fraction of the X-rays intercepted by the outer disk. The strength of the reprocessed component is thus scaled with $F_{\text{out}} = (1 - a_{\text{out}})f_{\text{out}}$.

References

- Axelsson, M., & Done, C. 2018, *Monthly Notices of the Royal Astronomical Society*, 480, 751
- Bohlin, R. C., Savage, B. D., & Drake, J. F. 1978, *The Astrophysical Journal*, 224, 132
- Burrows, D. N., Hill, J. E., Nousek, J. A., et al. 2005, *Space Science Reviews*, 120, 165
- Chiang, C. Y., Done, C., Still, M., & Godet, O. 2010, *Mon. Not. R. Astron. Soc.*, 403, 1102
- Corbel, S., Tomsick, J. A., & Tzioumis, T. 2014, *The Astronomer's Telegram*, No.5911, 5911
- Cunningham, C. 1976, *The Astrophysical Journal*, 208, 534
- Degenaar, N., Maitra, D., Cackett, E. M., et al. 2014, *The Astrophysical Journal*, Volume 784, Issue 2, article id. 122, 7 pp. (2014)., 784, arXiv:1403.0939
- Done, C., Davis, S. W., Jin, C., Blaes, O., & Ward, M. 2012, *Mon. Not. R. Astron. Soc.*, 420, 1848
- Done, C., Gierlí, M., Kubota, A., et al. 2007, *Astron Astrophys Rev*, 15, 1
- Done, C., Wardziński, G., & Gierliński, M. 2004, *Monthly Notices of the Royal Astronomical Society*, Volume 349, Issue 2, pp. 393-403., 349, 393
- Ebisawa, K., Makino, F., Mitsuda, K., et al. 1993, *The Astrophysical Journal*, 403, 684
- Esin, A. A., McClintock, J. E., & Narayan, R. 1997, *The Astrophysical Journal*, 489, 865
- Fender, R., Gallo, E., & Jonker, P. 2004a, in *Nuclear Physics B - Proceedings Supplements*, Vol. 132, 346–353
- Fender, R. P. 2001, *Mon. Not. R. Astron. Soc.*, 322, 31
- Fender, R. P., Belloni, T. M., & Gallo, E. 2004b, *Mon. Not. R. Astron. Soc.*, 355, 1105
- Fender, R. P., Hjellming, R. M., Tilanus, R. P. J., et al. 2001, *Mon. Not. R. Astron. Soc.*, 322, 23
- Filippova, E., Bozzo, E., & Ferrigno, C. 2014, *A&A*, 563, doi:10.1051/0004-6361/201323337
- Frank, J., King, A., & Raine, D. 1992, *Accretion Power in Astrophysics* (2nd ed.; Cambridge: Cambridge Univ. Press), 21
- Fukazawa, Y., Mizuno, T., Watanabe, S., et al. 2009, *Publications of the Astronomical Society of Japan*, 61, S17
- Gehrels, N., Chincarini, G., Giommi, P., et al. 2004, *The Astrophysical Journal*, 611, 1005
- Gierlinski, M., & Done, C. 2003, *Monthly Notice of the Royal Astronomical Society*, Volume 342, Issue 4, pp. 1083-1092., 342, 1083
- Gierlinski, M., Zdziarski, A. A., Poutanen, J., et al. 1999, *Monthly Notices*, Volume 309, Issue 2, pp. 496-512., 309, 496
- Gierlinski, M., Done, C., & Page, K. 2008, *Mon. Not. R. Astron. Soc.*, 388, 753
- . 2009, *Mon. Not. R. Astron. Soc.*, 392, 1106
- Grebenev, S. A., Prosvetov, A. V., Burenin, R. A., Krivonos, R. A., & Mescheryakov, A. V. 2016, *Astronomy Letters*, Volume 42, Issue 2, pp.69-81, 42, 69
- Heil, L. M., Uttley, P., & Klein-Wolt, M. 2015, *MNRAS*, 448, 3339
- Homan, J., & Belloni, T. 2005, *Astrophysics and Space Science*, 300, 107
- Hori, T., Ueda, Y., Shidatsu, M., et al. 2014, *The Astrophysical Journal*, doi:10.1088/0004-637X/790/1/20
- Kawabata, K. S., Nagae, O., Chiyonobu, S., et al. 2008, in *Ground-based and Airborne Instrumentation for Astronomy II*. Edited by McLean, Ian S.; Casali, Mark M. *Proceedings of the SPIE*, Volume 7014, article id. 70144L, 10 pp. (2008)., ed. I. S. McLean & M. M. Casali, Vol. 7014, 70144L
- Kawano, T., Done, C., Yamada, S., et al. 2017, *PASJ: Publ. Astron. Soc. Japan*, 69, 36(1)
- Kennea, J. A., Linares, M., Krimm, H. A., et al. 2013a, *The Astronomer's*

- Telegram, No.5478, 5478
- . 2013b, The Astronomer's Telegram, No.5479, 5479
- Kimura, M., & Done, C. 2018, Time-Evolved X-ray Irradiation during the 1999-2000 Outburst of the Black-Hole Binary XTE J1859+226, Tech. rep., arXiv:1808.02944v2
- Kimura, M., Isogai, K., Kato, T., et al. 2016, Nature, Volume 529, Issue 7584, pp. 54-58 (2016)., 529, 54
- Kobayashi, S. B., Nakazawa, K., & Makishima, K. 2017, Publications of the Astronomical Society of Japan, Volume 69, Issue 1, id.4 11 pp., 69, arXiv:1610.06333
- Kolehmainen, M., Done, C., & Trigo, M. D. 2011, Mon. Not. R. Astron. Soc, 416, 311
- Koyama, K., Tsunemi, H., Dotani, T., et al. 2007, PASJ: Publ. Astron. Soc. Japan, 59, 23
- Krivonos, R., & Tsygankov, S. 2013, The Astronomer's Telegram, No.5492, 5492
- Kubota, A., & Makishima, K. 2004, The Astrophysical Journal, 601, 428
- Kubota, A., Makishima, K., & Ebisawa, K. 2001, The Astrophysical Journal, 560, 147
- Kubota, A., Tanaka, Y., Makishima, K., et al. 1998, Publications of the Astronomical Society of Japan, 50, 667
- Laor, A. 1991, The Astrophysical Journal, 376, 90
- Li, L.-X., Zimmerman, E. R., Narayan, R., & McClintock, J. E. 2005, The Astrophysical Journal Supplement Series, 157, 335
- Maccarone, T. J. 2003, A&A, 409, 697
- Magdziarz, P., & Zdziarski, A. A. 1995, Mon. Not. R. Astron. Soc, 273, 837
- Mahmoud, R. D., & Done, C. 2018, Monthly Notices of the Royal Astronomical Society, Volume 473, Issue 2, p.2084-2097, 473, 2084
- Makishima, K. 2014, 40th COSPAR Scientific Assembly. Held 2-10 August 2014, in Moscow, Russia, Abstract id. E1.1-1-14., 40
- Makishima, K., Maejima, Y., & Mitsuda, K. 1986, The Astrophysical Journal, 308, 635
- Makishima, K., Takahashi, H., Yamada, S. y., et al. 2008, PASJ: Publ. Astron. Soc. Japan, 60, 585
- Markoff, S., Nowak, M. A., & Wilms, J. 2005, ApJ, 635, 1203
- Matsuoka, M., Kawasaki, K., Ueno, S., et al. 2009, PASJ: Publ. Astron. Soc. Japan, 61, 999
- Matt, G., Perola, G. C., & Piro, L. 1991, Astronomy and Astrophysics, 247, 25
- McClintock, J. E., & Remillard, R. A. 2006, Black hole binaries, ed. W. H. G. Lewin & M. van der Klis, 157213, arXiv:0306213
- Mihara, T., Nakajima, M., Sugizaki, M., et al. 2011, PASJ: Publ. Astron. Soc. Japan, 63, 623
- Miller, J. M., Raymond, J., Fabian, A. C., et al. 2006, Nature, Volume 441, Issue 7096, pp. 953-955 (2006)., 441, 953
- Miller-Jones, J. C. A., Russell, T. D., Sivakoff, G. R., & Curran, P. A. 2013, The Astronomer's Telegram, No.5484, 5484
- Mitsuda, K., Inoue, H., Koyama, K., et al. 1984, Astronomical Society of Japan, Publications (ISSN 0004-6264), vol. 36, no. 4, 1984, p. 741-759., 36, 741
- Mitsuda, K., Bautz, M., Inoue, H., et al. 2007, PASJ: Publ. Astron. Soc. Japan, 59, 1
- Nakahira, S., Negoro, H., Shidatsu, M., et al. 2014, PASJ: Publ. Astron. Soc. Japan, 66, 84(1)
- Nakahira, S., Koyama, S., Ueda, Y., et al. 2012, PASJ: Publ. Astron. Soc. Japan, 64, 13(1)
- Nakahira, S., Tomida, H., Negoro, H., et al. 2013, The Astronomer's Telegram, No.5474, 5474
- Negoro, H., Sugizaki, M., Mihara, T., et al. 2013, The Astronomer's Telegram, No.5483, 5483
- Negoro, H., Kohama, M., Serino, M., et al. 2016, Publications of the Astronomical Society of Japan, 68, S1
- Noda, H., Makishima, K., Nakazawa, K., et al. 2013, Publications of the Astronomical Society of Japan, Vol.65, No.1, article id.4, 18 pp., 65, arXiv:1208.3536
- Novikov, I. D., & Thorne, K. S. 1973, Black holes (Les astres occlus), p. 343-450. Edited by C. DeWitt and B. DeWitt, Gordon and Breach, N.Y., 343
- Plant, D. S., Fender, R. P., Ponti, G., Muñoz-Darias, T., & Coriat, M. 2014, MNRAS, 442, 1767
- Ponti, G., Fender, R. P., Begelman, M. C., et al. 2012, Monthly Notices of the Royal Astronomical Society: Letters, Volume 422, Issue 1, pp. L11-L15., 422, L11
- Poutanen, J. 1998, in Theory of Black Hole Accretion Disks, ed. M. A. Abramowicz, G. Björnsson, & J. E. Pringle, 100-122
- Poutanen, J., & Svensson, R. 1996, Astrophysical Journal v.470, p.249, 470, 249
- Rahoui, F., Coriat, M., Corbel, S., et al. 2012, Mon. Not. R. Astron. Soc, 422, 2202
- Rau, A., Tanga, M., & Greiner, J. 2013, The Astronomer's Telegram, No.5482, 5482
- Reig, P., & Kylafis, N. D. 2015, A&A, 584, A109
- Reig, P., Kylafis, N. D., & Giannios, D. 2003, A&A, 403, L15
- Reis, R. C., Fabian, A. C., & Miller, J. M. 2010, Monthly Notices of the Royal Astronomical Society, 402, 836
- Roming, P. W. A., Kennedy, T. E., Mason, K. O., et al. 2005, Space Science Reviews, 120, 95
- Sakurai, S., Torii, S., Noda, H., et al. 2014, PASJ, 66, 10
- Shakura, N. I., & Sunyaev, R. A. 1973, Astronomy and Astrophysics, Vol. 24, p. 337 - 355, 24, 337
- Shaw, A. W., Gandhi, P., Altamirano, D., et al. 2016, Monthly Notices of the Royal Astronomical Society, Volume 458, Issue 2, p.1636-1644, 458, 1636
- Shidatsu, M., Done, C., & Ueda, Y. 2016, The Astrophysical Journal, doi:10.3847/0004-637X/823/2/159
- Shidatsu, M., Ueda, Y., Tazaki, F., et al. 2011, PASJ: Publ. Astron. Soc. Japan, 63, 785
- Shidatsu, M., Ueda, Y., Nakahira, S., et al. 2013, The Astrophysical Journal, 779, doi:10.1088/0004-637X/779/1/26
- Shimura, T., & Takahara, F. 1995, The Astrophysical Journal, 445, 780
- Sobolewska, M. A., Papadakis, I. E., Done, C., & Malzac, J. 2011, Monthly Notices of the Royal Astronomical Society, Volume 417, Issue 1, pp. 280-288., 417, 280
- Steiner, J. F., McClintock, J. E., Remillard, R. A., et al. 2010, The Astrophysical Journal Letters, 718, 117
- Sugimoto, J., Mihara, T., Kitamoto, S., et al. 2016, Publications of the Astronomical Society of Japan, Volume 68, Issue SP1, id.S17 17 pp., 68, arXiv:1601.02740
- Sutton, A. D., Done, C., & Roberts, T. P. 2014, MNRAS, 444, 2415
- Takahashi, H., Fukazawa, Y., Mizuno, T., et al. 2008, PASJ: Publ. Astron. Soc. Japan, 60, 69
- Takahashi, T., Abe, K., Endo, M., et al. 2007, PASJ: Publ. Astron. Soc. Japan, 59, 35
- Tamura, M., Kubota, A., Yamada, S., et al. 2012, The Astrophysical Journal, 753, doi:10.1088/0004-637X/753/1/65

- Titarchuk, L., & Lev. 1994, *The Astrophysical Journal*, 434, 570
- Tomsick, J. A., & Corbel, S. 2014, *The Astronomer's Telegram*, No.5886, 5886
- Tomsick, J. A., Yamaoka, K., Corbel, S., et al. 2009, *The Astrophysical Journal Letters*, 707, L87
- Turon, C., M A C Perryman, Priou, D., & European Space Agency. 1998, *Celestia 2000 computer file : the Hipparcos and Tycho catalogues*, Vol. 1220 (ESA Publications Division)
- Turon, C., Cr ez e, M., Egret, D., et al. 1992, *The HIPPARCOS input catalogue*, Vol. 1136 (ESA Publications Division)
- Ueda, Y., Yamaoka, K., & Remillard, R. 2009, *The Astrophysical Journal*, Volume 695, Issue 2, pp. 888-899 (2009)., 695, 888
- Vaughan, S., Edelson, R., Warwick, R. S., & Uttley, P. 2003, *Monthly Notices of the Royal Astronomical Society*, Volume 345, Issue 4, pp. 1271-1284., 345, 1271
- Wang, S., Kawai, N., Shidatsu, M., et al. 2018, *Publications of the Astronomical Society of Japan*, Volume 70, Issue 4, id.67, 70, arXiv:1808.04775
- Wilms, J., Allen, A., & McCray, R. 2000, *THE ASTROPHYSICAL JOURNAL*, 542, 914
- Winkler, C., Courvoisier, .-L., Di Cocco, G., et al. 2003, *A&A*, 411, 1
- Yamada, S., Makishima, K., Done, C., et al. 2013, *PASJ: Publ. Astron. Soc. Japan*, 65, 80(1)
- Yamada, S., Uchiyama, H., Dotani, T., et al. 2012, *PASJ: Publ. Astron. Soc. Japan*, 64, 53
- Zdziarski, A. A., Neil Lohson, W., & Magdziarz, P. 1996, *Mon. Not. R. Astron. Soc.*, 283, 193
- Zdziarski, A. A., Poutanen, J., Mikolajewska, J., et al. 1998, *MNRAS*, 301, 435
- Zhang, Z., Sakurai, S., Makishima, K., et al. 2016, *The Astrophysical Journal*, 823, doi:10.3847/0004-637X/823/2/131
- Życki, P. T., Done, C., & Smith, D. A. 1999, *Monthly Notices*, 309, 561